CrossMark

Development of a powered variable-stiffness exoskeleton device for elbow rehabilitation

Yi Liu[1] · Shuxiang Guo[2,3] · Hideyuki Hirata[3] · Hidenori Ishihara[3] · Takashi Tamiya[4]

Abstract

Robot-assisted movement training by means of exoskeleton devices has been proven to be an effective method for post-stroke patients to recover their motor function. However, in order to be used in home-based rehabilitation, the kinematic structure of a wearable exoskeleton device should provide portability and make allowances for the natural joint range of motion for the user. Additionally, the actuated stiffness of the target joint is desired to be adjustable in accordance with the specific impairment level of the patient's upper limb. In this paper, we present a novel portable exoskeleton device which could provide support for rehabilitation patients with variable actuated stiffness in the elbow joint. It has five passive degrees of freedom to guarantee the user's natural joint range of motion and intra-subject variability, as well as an integrated variable stiffness actuator (VSA) which can adjust the joint stiffness independently by moving the pivot position. An elbow power-assist trial with different actuated joint stiffnesses was tested on a healthy subject to evaluate the functionality of the proposed device. By regulating the joint stiffness, the proposed device could provide variable power assistance for the wearer's elbow movements.

Keywords Rehabilitation device · Portability · Variable stiffness actuator · Elbow rehabilitation

1 Introduction

A report from the American Heart Association shows that the incidence rate of stroke has a sustained growth with the increase of aged population (Mozaffarian et al. 2016). Nearly 85% of stroke survivors experience difficulty in performing activities of daily living (ADLs), which results in a large demand for rehabilitation (Barreca et al. 2003). However, manual rehabilitation therapy requires intensive labor from physical therapists and consumes significant medical resources. In order to reduce this burden and provide a stable rehabilitation process for post-stroke patients, robot-aided rehabilitation training has been proposed (Babaiasl et al. 2016; Kwakkel et al. 2008; Norouzi-Gheidari et al. 2012). Compared with conventional manual therapy, robot-aided rehabilitation could provide intensive and repetitive movement training for the patients with severely impaired limbs (Lum et al. 2002). Moreover, the patients' motor functions can be precisely quantified by attaching embedded sensors (Vanpee et al. 2014). Clinical studies have claimed that robot-assisted movement training can significantly improve post-stroke patients' muscular strength (Hesse et al. 2003; Lo et al. 2010).

Passive rehabilitation training by the aid of rehabilitation devices is an effective way for post-stroke patients to recover impaired upper limbs (Maciejasz et al. 2014). In passive rehabilitation training, the device drives the user's upper limb to complete task-oriented movements. However, a proper actuated stiffness is needed to guarantee sufficient torque to perform predefined movements as well as a safe human-robot interaction. Although stiff actuation could provide enough torque to accomplish precise position control, a high actuated joint stiffness may cause discomforts and/or injuries to the wearer during the exercise, particularly, in the early stage of rehabilitation when stroke patients often suffer severe spasms,

✉ Yi Liu
s18d504@stu.kagawa-u.ac.jp

✉ Shuxiang Guo
guo@eng.kagawa-u.ac.jp

1   Graduate School of Engineering, Kagawa University, 2217-20 Hayashi-cho, Takamatsu, Kagawa 761-0396, Japan

2   Key Laboratory of Convergence Medical Engineering System and Healthcare Technology, the Ministry of Industry and Information Technology, Beijing Institute of Technology, No. 5, Zhongguancun South Street, Haidian District, Beijing 100081, China

3   Faculty of Engineering and Design, Kagawa University, 2217-20 Hayashi-cho, Takamatsu, Kagawa 761-0396, Japan

4   Department of Neurological Surgery, Faculty of Medicine, Kagawa University, 1750-1 Miki-cho, Takamatsu, Kagawa 761-0701, Japan

i.e., involuntary contractions of muscles. Undesired motions caused by spasms will force the upper limb to deviate from the predefined trajectory. These deviations would be inhibited during high joint stiffness thereby creating large interaction forces between human and exoskeletal joints, which would threaten the user's safety. Adding compliance to the actuation system could produce a lower actuated joint stiffness, which would allow deviations from the reference position and naturally absorbs the interaction force. Low joint stiffness can prevent potential injury to the user's limbs while improving wearing comfort at the expense of increasing position tracking errors (Wolf et al. 2016). Series elastic actuators (SEAs) use a spring in series with a stiff actuator to generate the compliance of the actuation system. They were widely applied in rehabilitation devices in order to ensure a safe and comfortable human-robot interaction during the rehabilitation process (Song et al. 2014; Yu et al. 2013; Zhang et al. 2014). However, the physical compliance of SEAs is a fixed value related to the coefficient of the spring elasticity. Only by means of complicated closed-loop interaction control strategies could its physical stiffness be regulated (Li et al. 2017; Yu et al. 2015).

For a rehabilitation device focused on passive rehabilitation training, the actuated stiffness of the target joint should be adjustable in accordance with the specific impairment level of the patient's upper limb (Van Ham et al. 2009). A relative low actuated joint stiffness is recommended for those patients with severely impaired arms to minimize large interaction forces and to prevent further injuries. When patients regain partial control of their upper limbs, the actuated joint stiffness is supposed to be gradually increased to achieve higher position tracking accuracy as well as improving the training intensity.

Variable stiffness actuators (VSAs) have the ability to adjust the stiffness of the actuated link independently (Groothuis et al. 2014). The generated stiffness is an inherent hardware property without complicated closed-loop interaction control strategies (Visser et al. 2011). As a result, stiffness variation by means of VSAs can minimize the risk of instabilities caused by the control system. Rehabilitation devices equipped with a VSA could provide different levels of assistance in accordance with the specific impairment level of the patient's upper limb and gradually promote the intensity of rehabilitation training. This characteristic has positive effects on recovering neurological motor function, especially for chronic hemiparetic stroke survivors (Patton et al. 2006).

In this paper, a novel powered variable-stiffness exoskeleton device (PVSED) is presented for safe and convenient elbow rehabilitation. The following sections of this paper are organized to elaborate on the characteristics of the proposed device. Mechanical design, control system and kinematic analysis are described in Section 2. In Section 3, the working principle of the integrated VSA is presented in detail. In Section 4, the characteristic of the integrated VSA and the functionality of the proposed PVSED are evaluated through experimentation. Comparisons with other exoskeleton devices and expected functions are discussed in Section 5. Finally, conclusions and future work are given in Section 6.

2 Method

2.1 Mechanical design

The mechanical design of the proposed PVSED is seen in Fig. 1. The device mainly consists of a back section, an adjustable upper limb section integrated with a VSA and several joint parts which are used to connect the back section and the upper limb section. A control board (No. 1) and a battery pack (No. 4) are mounted on the back section to achieve fully portable application. The PVSED is equipped with a compact DC motor (No. 3) which provides power assistance for elbow movements. In order to reduce the inertia to the human joints, the power motor is fixed to the back section, away from the upper limb joints, and uses pulleys and cables (No. 2) to drive the exoskeleton device. There is a belt and two shoulder straps (No. 10) which allows the wearer to carry the device on his/her back much like carrying a backpack. The elbow joint (No. 12) is connected with the driving cable. A VSA is integrated into the forearm and can be used to adjust the elbow joint stiffness independently. It mainly consists of a pair of antagonist elastic elements (No. 13), a slider (No. 14) along with a movable pivot, a forearm supporter (No. 15), and a DC motor (No. 16).

A physical model of the PVSED when worn is shown in Fig. 2. As a wearable rehabilitation device designed for home-based rehabilitation, the PVSED has a light and compact mechanical structure. The main exoskeletal frames are made of aluminum alloys and several connection parts were manufactured by a 3D printer to reduce the weight as well as the cost. The total weight of the PVSED is only 3.1 kg. The motors and control boards are supplied by a rechargeable battery pack with a capacity of 3000 mAh, which could allow nearly 1 h of continuous elbow rehabilitation training. These features help facilitate home-based rehabilitation but also allows for its use outside of the home.

A notable characteristic of the proposed PVSED is that the elbow joint could be powered with variable joint stiffnesses. A pair of antagonist cables with a diameter of 1.2 mm connected to the driving pulley is used to transmit the motor power to perform predefined movements. The diameter of the pulley connected to the driving motor is 46 mm, which is the same as the mounted pulley on the elbow joint of the device. As a result, the rotation angle of the driving motor is equal to the elbow joint rotation angle of the exoskeleton device. For the purpose of realizing different levels of movement assistance, a
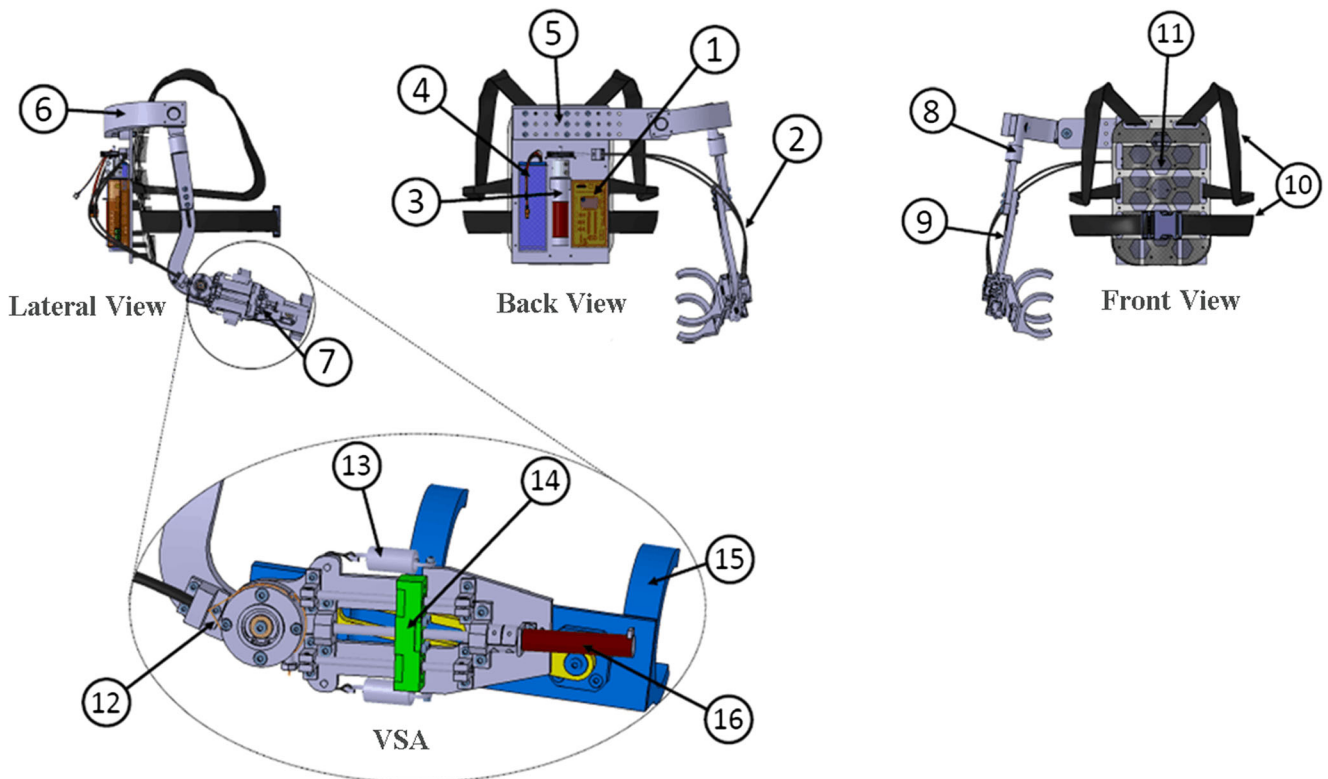
Fig. 1 Mechanical design of PVSED (1. Motor controller; 2. Cable; 3. Power motor; 4. Battery pack; 5. Adjustable back frame; 6. Shoulder frame; 7. VSA; 8. Internal/external rotational joint; 9. Adjustable upper limb frame; 10. Belt and straps; 11. Back supporter; 12. Elbow joint; 13. Spring; 14. Slider; 15. Forearm supporter; 16. VSA motor)

VSA is utilized to adjust the elbow joint stiffness independently. The physical prototype of the VSA is shown in Fig. 3. It mainly consists of a DC motor (Maxon RE-13 Graphite Brushes Motor), a pair of antagonistic springs, a ball screw, a slider, a main frame and an output link. A pair of springs is connected by steel cables and mounted on the main frame. The motor drives the ball screw to move the slider along with the pivot. The output link worn by the user and the main frame driven by cables are linked together through a shaft mounted on the elbow joint. By moving the slider to change the pivot position, the transmission ratio between the output force and the spring force can be adjusted thereby leading to an apparent variation of the output stiffness.

2.2 Actuation, control and sensory apparatus

The elbow movement is powered by a Maxon RE-30 Graphite Brushes Motor. A Maxon Planetary Gearhead GP 32C
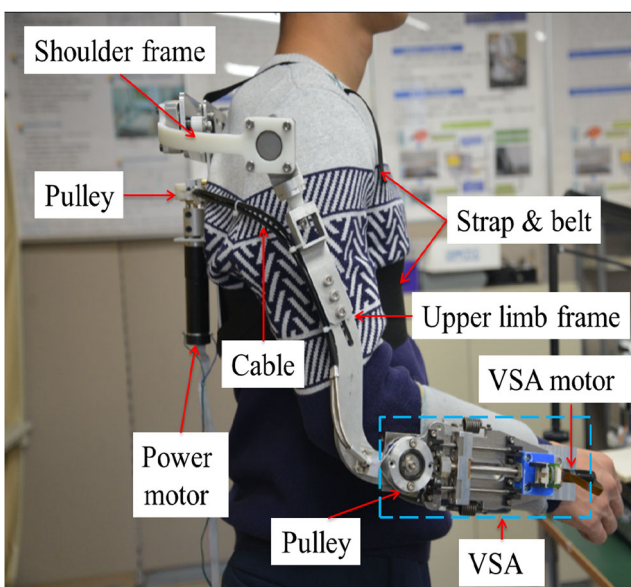

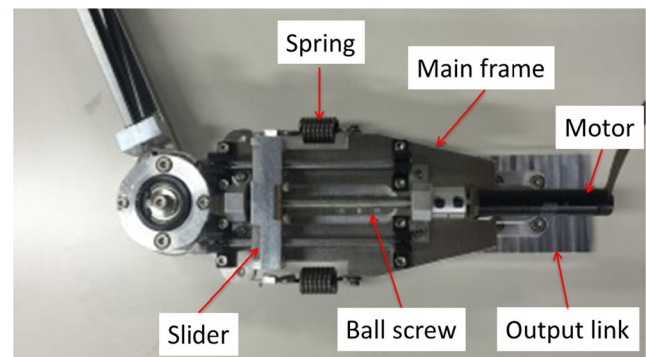**Fig. 2** Physical model of PVSED with a wearer

Fig. 3 Physical prototype of the integrated VSA

gearhead with a reduction ratio of 190:1 is assembled with the motor. They are mounted on the back section of the exoskeleton device. In order to control the device, sensors are required to measure the states of the motors. The rotation angle of the driving motor is measured by an incremental optical encoder (Maxon MR L-512, Maxon Motor AG, Switzerland) which is assembled with the driving motor concentrically. The encoder has 512 counts per revolution. The rotation angle of the driving motor can be obtained by

$$\theta = c \cdot \frac{360}{512*190} \quad (1)$$

where

θ is the rotation angle of the driving motor and
c   is the number of counts from its initial position recorded by the encoder.

Therefore, the rotation angle of the driving motor is represented by the number of counts c thus acquiring the elbow rotation angle. A compact angle sensor (GY-25) with a resolution of 0.01° is attached to the elbow joint of the device to measure the actual rotation angle of the elbow and provide feedback to the controller for realizing a closed-loop position control of the elbow joint.

The actuated joint stiffness of rehabilitation devices should be adjustable to adapt to those users with different impairment levels of the upper limbs. In the proposed PVSED, we apply a VSA to regulate the actuated elbow joint stiffness. A Maxon RE-13 Graphite Brushes Motor is equipped in the VSA to drive the ball screw for moving the pivot position. The helical pitch of the ball screw is 1 mm. A Maxon Planetary Gearhead GP 13A gearhead with a reduction ratio is 67:1 is assembled with the motor. Additionally, a Maxon MR L-256 incremental optical encoder with 256 counts per revolution is used to measure the current count number of the motor. Therefore, the pivot position can be obtained by

$$d = c \cdot \frac{1}{256*67} \quad (2)$$

where

d   is the pivot position and
c   is the number of counts from its initial position recorded by the encoder.

The parameters of the aforementioned motors and gearheads can be found in Table 1 and Table 2 respectively. For the control system, it should achieve desired movements while avoiding potential risks caused by the device. Arduino Mega 2560 (Arduino, Italy), as the embedded control unit of the device, is used to regulate the elbow rotation and pivot position by sending corresponding orders to the motor controller. Both of the two motors are controlled by a 50/5

Table 1   Motor parameters

Motor	RE-30	RE-13
Diameter	30 mm	13 mm
Motor length	88 mm	40.5 mm
Weight	260 g	27 g
Type power	60 W	3 W
Nominal voltage	12 V	18 V
No load speed	7480 rpm	13,000 rpm
Nominal torque	51.7 mNm	2.36 mNm

ESCON motor controller (Maxon Motor AG, Switzerland). To ensure the wearer's safety during movements, the GY-25 angle sensor measures the actual elbow angle with a frequency of 25 Hz. Once the measured elbow rotation difference is larger than 6° (i.e., the rotation speed is larger than 150°/s), the control system will switch off the actuation immediately. Based on the use of the efficient DC motors and the embedded control unit, a compact actuation system is accomplished in the proposed PVSED.

2.3 Kinematic analysis

As shown in Fig. 4, the PVSED has 6 degrees of freedom (DOFs) including 3 human-motion controlled passive DOFs which can be rotated freely to cater to the patients' active movements, two passive length adjustment DOFs to fit different body sizes and 1 active elbow DOF actuated by the motor. The motions of the shoulder joint are complicated for the reason that the position of the center of the glenohumeral joint would be varied during the shoulder movements, which can cause the misalignment of the exoskeletal joint axes with the human joint axes. This misalignment can be reduced by adding passive or active DOFs at the shoulder (Nef et al. 2009). 3 passive shoulder DOFs including shoulder adduction/ abduction, shoulder flexion/extension and internal/external rotation of the upper limb are designed for the proposed device to minimize this misalignment. The main frame lengths of the PVSED can be adjusted by 2 DOFs on the

Table 2   Gearhead parameters

Gearhead	GP 32 C	GP 13 A
Reduction	190:1	67:1
Diameter	32 mm	13 mm
Gearhead length	43.1 mm	23.7 mm
Max. continuous torque	6 Nm	0.3 Nm
Max. efficiency	70%	75%

Fig. 4 Kinematic model of PVSED. The 6 DOFs are labeled by number 1–6 respectively, where 1. Back frame adjustment; 2. Shoulder adduction/abduction; 3. Shoulder flexion/extension; 4. Internal/external rotation of the upper limb; 5. Upper limb frame adjustment; 6. Elbow flexion/extension, active DOF
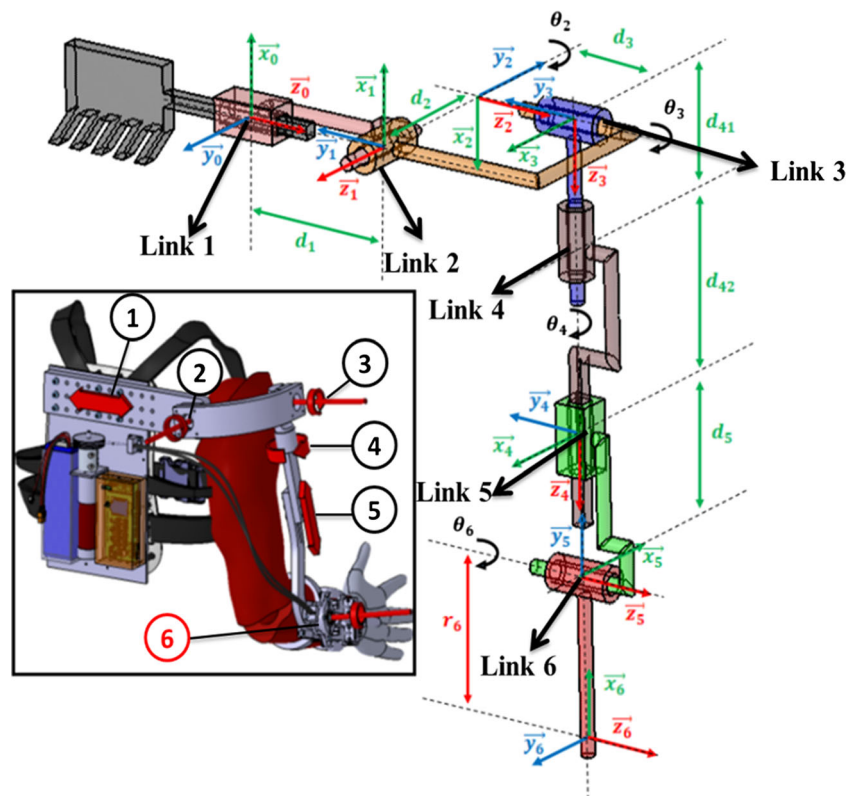
back frame and the upper limb frame. The back frame can adjust the shoulder breadth in the range of 300–450 mm, while the upper limb frame can adjust the shoulder-elbow length in the range of 250–380 mm. As a result, the PVSED is capable of providing optimal link lengths for people with different body sizes. Moreover, there is an active DOF powered by the motor to assist elbow movements via cables.

The kinematic structure of a wearable rehabilitation device should take into account the subject's natural joint range of motion (ROM) and the intra-subject variability of the body size (Stienen et al. 2009). Denavit-Hartenberg (D-H) parameters draw an available methodology for the kinematic analysis of robotic systems. With this method, each link frame is completely described by four parameters associated with a convention matrix (Siciliano and Khatib 2016). For the proposed PVSED, the coordinate frames from link 1 to link 6 are established and shown in Fig. 4. The position of the first link can be moved to adjust the base frame to a suitable position and avoid the interference between the exoskeletal and human joints. Link 2–4 are 3 passive revolute joints designed to fit the subject's shoulder joint movements. The position of Link 5 can be adjusted to guarantee an accurate alignment with the human elbow joint. Finally, Link 6 is the actuated end effector to perform elbow flexion and extension via cables. Based on the established coordinate frames, D-H parameters for each link are listed in Table 3. Among these parameters, θ_2, θ_3,

θ_4 and θ_6 represent the parameters of the different rotational joints that allow patients to move their arm in all directions, while d_1 and d_5 are the parameters of prismatic joints which are used to adjust the link length.

To explore the maximum available area when using the device, we assume the passive shoulder DOFs are moved by human power while the elbow DOF is actuated by the cable-driven PVSED. The available movement range is described in Fig. 5 and its target ROM of the revolute joints is seen in Table 4. To prevent any robot-driven movements exceeding the ROM of human joints, the joint ROM of the PVSED is limited to be slightly smaller than that of human joints but its range meets most requirements of ADLs (Perry et al. 2007).

Table 3   D-H parameters

Link	θ_i	d_i	r_i	α_i
1	0	d_1(JV)	0	$-\pi/2$
2	$\pi + \theta_2$(JV)	d_2	0	$-\pi/2$
3	$-\pi/2 + \theta_3$(JV)	d_3	0	$-\pi/2$
4	θ_4(JV)	$d_{41} + d_{42}$	0	0
5	π	d_5(JV)	0	$-\pi/2$
6*	θ_6(JV)	0	r_6	0

JV: Joint Variable; Link 1–5 are passive joints, Link 6* is the active joint actuated by the motor

Fig. 5 Available area (**a**) Schematic diagram of the available area; (**b**) Computed available area
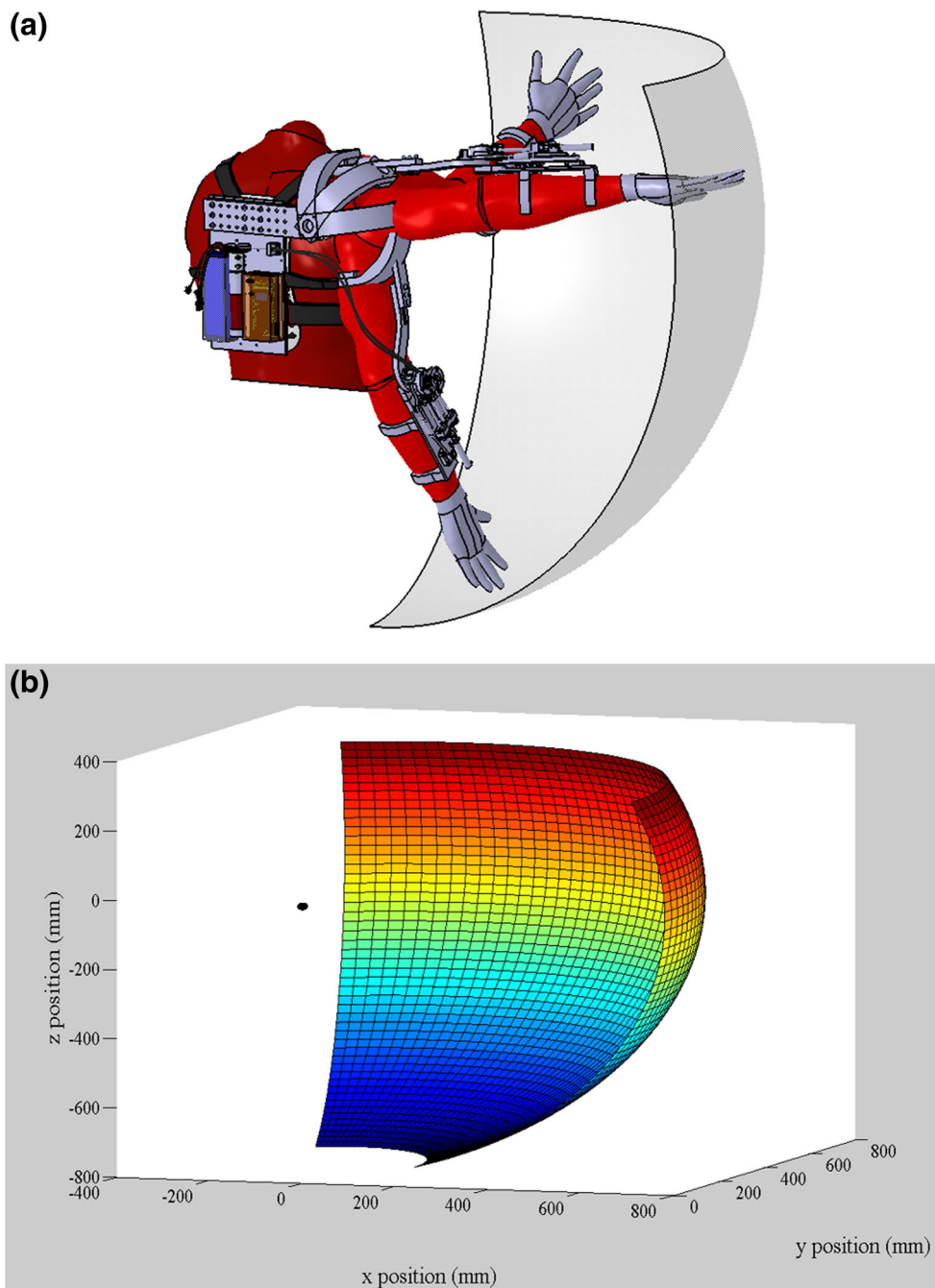
3 Principle of variable stiffness and simulation

3.1 Principle of variable stiffness

The conceptual scheme of the proposed VSA is seen in Fig. 6. There is an actuated load at the end of the lever, while the other side is tensioned with a pair of antagonistic springs via steel cables. Due to spring elongation, the force exerted at the end of the lever can be balanced. As long as the pivot position is changed, the transmission ratio between the exerted load and the antagonistic forces generated by the elastic elements would be changed as well thereby allowing the variation of the output stiffness. As a result, the stiffness variation is an inherent property with respect to the pivot position.

The working principle of the VSA is explained by Fig. 7. In this figure, O is the revolution axis mounted on the elbow joint of the device. P is the pivot which can be moved along the lever arm with a movable range of RH. AM and BM' represent the cables which are connected with elastic elements. When the external force is exerted at the end of the output

Table 4 Target joint range of motion

Joint	Motion	Range
Shoulder (Passive)	abduction/adduction (θ_2)	[0°, 90°]
	flexion/extension (θ_3)	[−45°, 125°]
	Internal/external rotation (θ_4)	[−80°, 70°]
Elbow (Active)	flexion/extension (θ_6)	[0°, 135°]

Passive: rotation controlled by human motions; Active: rotation controlled by the motor

link, one of the springs will be elongated thereby generating an elastic force to balance the exerted force.

Based on the equilibrium of moments $\sum M = 0$,

$$F_{exert} \cdot \cos(\beta - \alpha) \cdot L_2 - F_{spring} \cdot \cos\gamma \cdot L_1 = 0 \qquad (3)$$

where

L_1 is the distance from the spring side AB to the pivot P, while
L_2 is the distance from the actuated load D to the pivot P.
α is the deflection angle of the movable forearm part and
β is the rotation angle of the lever arm about the pivot P.
γ is obtained by projecting the spring force vector along the direction of CB as shown in Fig. 7.

According to Hooke's law,

$$F_{spring} = k_{spring} \cdot \Delta \qquad (4)$$

where k_{spring} is the elastic coefficient and Δ is the elongation of the spring. In this mechanism, we selected the spring with an elasticity coefficient of 19.6 N/mm.

By substituting Eq. (4) in (3), the exerted force is described as follows:

$$F_{exert} = \frac{\left(k_{spring} \cdot \Delta \cdot \cos\gamma \cdot L_1\right)}{L_2 \cdot \cos(\beta - \alpha)} \qquad (5)$$
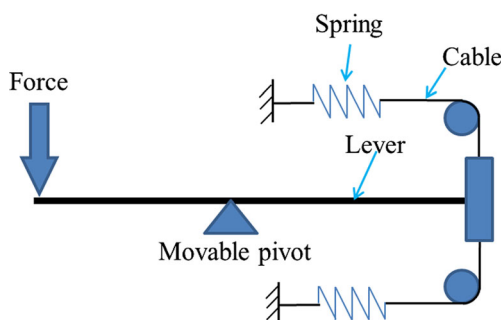

Fig. 6 Schematic of the proposed VSA. The pivot can be moved along the lever to adjust the transmission ratio between the spring and the exerted force

The joint stiffness, defined as $K = \partial F / \partial \alpha$, is represented by

$$K = \frac{\partial F}{\partial \alpha} = \frac{\left(k_{spring} \cdot \Delta \cdot \cos\gamma\right)}{\alpha \cdot \cos(\beta - \alpha)} \cdot \frac{L_1}{L_2} \qquad (6)$$

where

K is the output stiffness,
F is the force exerted at the end of the output link and
α is the output deflection angle with respect to its original equilibrium position.

As Eq. (6) indicates, the output stiffness mainly relies on the transmission ratio L_1/L_2. By adjusting the pivot position along the lever arm to change the transmission ratio L_1/L_2, different stiffness settings can be achieved as shown in Fig. 8.

3.2 Simulation protocol and results

Five pivot positions were selected to simulate its corresponding elbow joint stiffness respectively. The first pivot position is located at the start position of the ball screw as shown in Fig. 9 and defined as 0 mm. A force is exerted at the end of output link from 0 N to 25 N with a constant increment of 1 N per second. The friction and gravity were neglected for simplification. The original equilibrium position is shown in Fig. 9 (a) and the deflection angle is defined as the deviation of the output link from its original equilibrium position. It can be observed that the deflection angle between the main frame and the output link becomes larger with the increase of simulated force.

The simulation results along with the linear fit for the pivot position at 0 mm are seen in Fig. 10. The fitted deflection-force relationship is represented by

$$\theta = 1.0677 * F + 0.4676 \ (0 \ N \leq F \leq 25 \ N) \qquad (7)$$

According to the definition, the rotational stiffness is given by

$$K = \frac{T}{\delta} \qquad (8)$$

where

T is the applied torque,
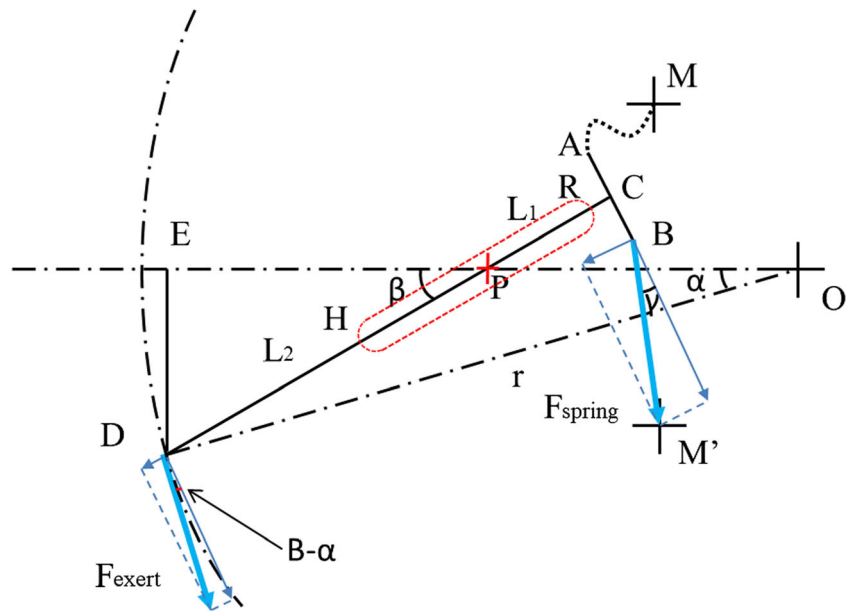δ is the radian with respect to its initial position.

Hence, the elbow joint stiffness is measured by

$$K = \frac{F \cdot L}{\theta} \cdot \frac{180}{\pi} \qquad (9)$$

where

F is the applied force,
θ is the deflection angle, and
L is the length of the lever which is equal to 215 mm.

Fig. 7 Schematic of the working principle

The other four pivot positions were selected successively with an increment of 5 mm (i.e., [5 mm, 10 mm, 15 mm, 20 mm]). The simulations were repeated using the new pivot position with the same simulation settings. The stiffness for all five different pivot positions is derived from the simulation results and reported in Table 5. It can be seen that the stiffness of elbow joint becomes significantly higher by increasing the pivot position.

Fig. 8 Schematic diagram of different stiffness settings by moving the pivot position. (a) Low stiffness (b) High stiffness

4 Experiments and characteristic evaluations

4.1 Characterization of the VSA

To characterize the proposed VSA, we carried out experiments to derive the output stiffness for different pivot positions. The experimental setups are shown in Fig. 11. Firstly, the VSA is set on the equilibrium position where there was no deflection angle between the main frame and the output link. The main frame and the output link can be rotated together if there is no external force on the output link. In the experiment, the force of output link was measured by a 6-axis force sensor (MINI 4/20, BL AUTOTEC. Ltd.) with a maximum force measure capability of 80 N and a resolution of 0.04 N. An inertial sensor (MTx sensor, Xsens Technologies B.V., the Netherlands) with a resolution of 0.05° was attached to the elbow joint to measure the output deflection angle from its equilibrium position. The main frame was driven by cables to rotate from its equilibrium position, while the output link was blocked by the force sensor thus generating the deflection angle between the main frame and the output link. The interaction force and the deflection angle were recorded simultaneously to derive the output deflection-force diagram. To minimize the measurement errors resulting from the displacements during rotation, the exerted force was obtained by calculating the resultant force, i.e., $F = \sqrt{F_x^2 + F_y^2 + F_z^2}$. Five pivot positions, namely 0 mm, 5 mm, 10 mm, 15 mm, 20 mm, are the same with those selected in the simulation. The measurements were iterated 5 times for each pivot position in the positive direction (clockwise) and the negative direction (anticlockwise) respectively.
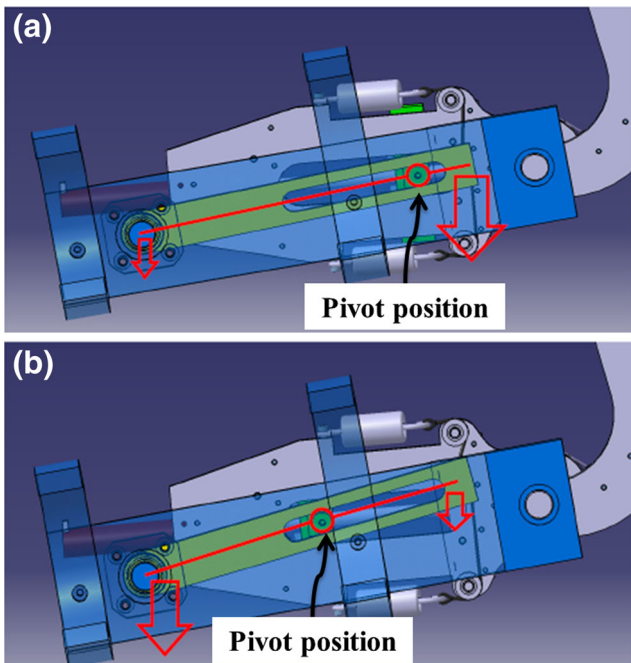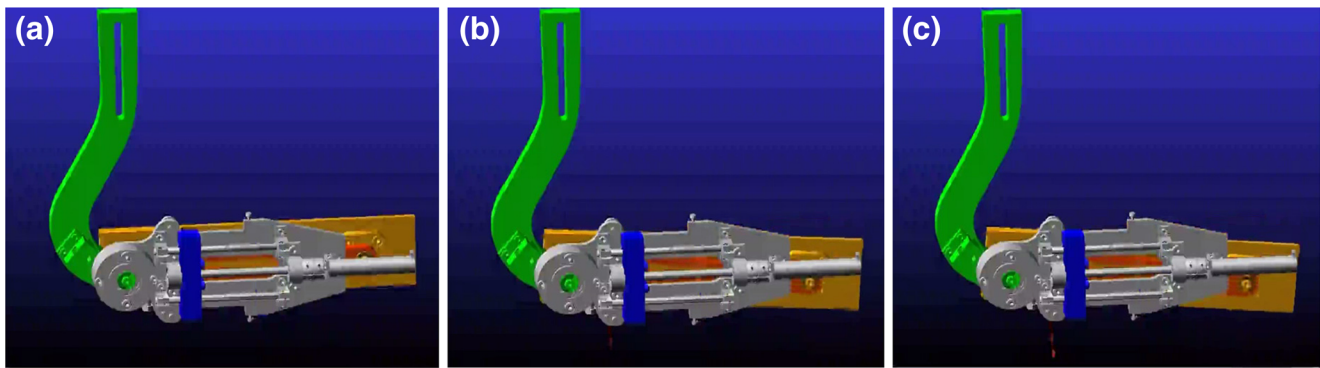
Fig. 9 Simulation process of pivot position at 0 mm. **a** Simulated force is 0 N. **b** Simulated force is 15 N. **c** Simulated force is 25 N. The deflection angle becomes larger with the increase of the simulated force

Figure 12 shows the experimental results of joint force versus deflection angle. The force-deflection curves for each pivot position were processed by a linear fitting method based on the principle of least-squares approximation. The dash lines represent the results of linear fitting for the five pivot positions. It can be observed that to rotate the same deflection angle, the measured force became larger with the increase of the pivot position. As Eq. (9) indicates, the slope of each curve is proportional to its stiffness. With the pivot position increased from 0 mm to 20 mm, the slope of force-deflection diagram became larger, which means a stiffer actuated elbow joint was achieved.

The joint stiffness measured by linear fitting and the root mean square error (RMSE) for each pivot position are reported in Table 6. By moving the pivot position from 0 mm to 20 mm, the measured elbow joint stiffness increased from 18 Nm/rad to 119 Nm/rad.

From the experimental results in Fig. 12, it can be seen that an inflection point of the slope appeared in the initial stage of each curve for both the positive and negative directions. The inflection point is caused by the internal backlash effect of the cable. Firstly, the slope difference at the inflection point is especially notable when the pivot position is small (this effect has a great influence on low joint stiffness). Secondly, the linearity of the deflection-force diagram is improved after the initial stage. By linearly approximating the portion of the curve after the inflection point, the compensated stiffness is reported in Table 7, where the decreased RMSE reveals an improved linearity of the force versus deflection relationship. Both of them indicate the inflection point results from the inherent characteristic of the physical cable-driven system.

In order to validate the VSA model and estimate the relationship between the pivot position and the elbow joint stiffness, the joint stiffness versus pivot position diagram is plotted in Fig. 13. Compared with the simulated stiffness, the measured stiffness is higher since the initial stage suffered the backlash effect caused by the driving cable in the experiment. The compensated stiffness curve shows an approximated value with the simulation results although there are small differences which resulted from the energy dissipation (e.g., friction) in the physical system. This indicates that the proposed model properly represents the stiffness property of the VSA. Although a more accurate approximation can be achieved by adding the insertion points of the pivot position, all three of the curves in Fig. 13 show a significant tendency for the actuated joint stiffness to become higher with the increase of the pivot position. The elbow joint stiffness is supposed to be increased with a larger pivot position, but considering the available range of the human elbow joint stiffness for upper limb movements (Abe and Yamada 2003), the current variation range of stiffness can meet the requirements of passive rehabilitation training.
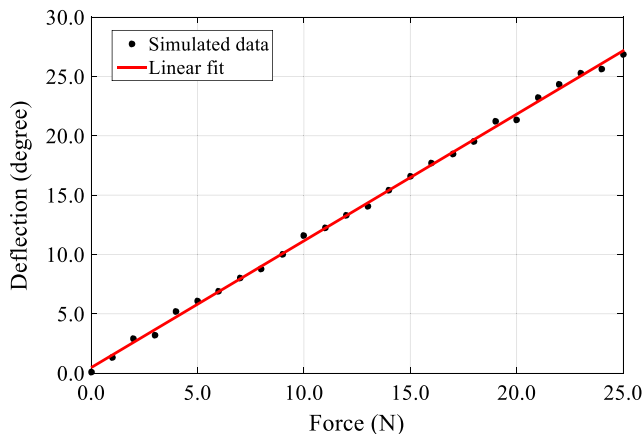

Fig. 10 Simulation results of the pivot position at 0 mm

Table 5 Simulated stiffness K

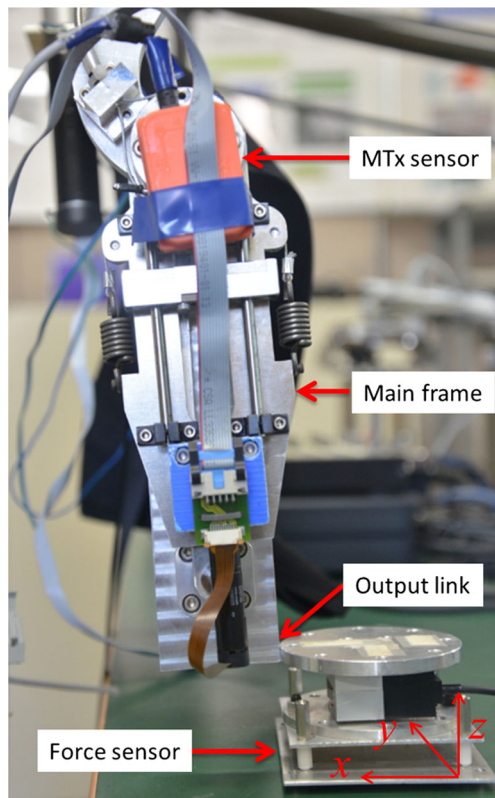| Pivot Position d (mm)	Simulated K (Nm/rad)
0	11.53
5	18.48
10	40.65
15	71.43
20	107.17

Fig. 11 Experimental setups. The output link is blocked by the force sensor, and the deflection angle is measured by the Mtx sensor attached to the elbow joint

4.2 Functional evaluation

To evaluate the functionality of the proposed PVSED, elbow power-assist experiments were tested on a healthy subject (Male, 28 years old, 175 cm, 67 kg). Before the experiments, the subject signed an informed consent and this study was
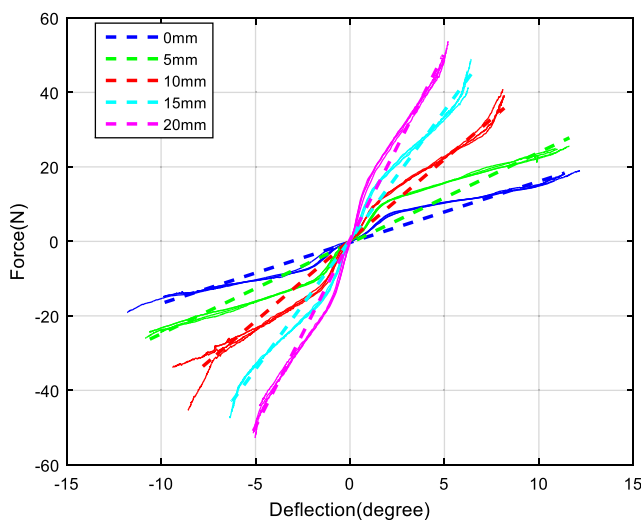

Fig. 12 Joint force versus deflection angle for the five different pivot positions. The dashed lines show the linear fitting results

Table 6 Measured stiffness K

Pivot Position d (mm)	Measured K (Nm/rad)	RMSE (Nm/rad)
0	18.48	4.97
5	28.33	6.35
10	56.05	4.21
15	84.99	3.12
20	119.49	2.85

approved by the Institutional Review Board (IRB) at Faculty of Medicine, Kagawa University. During the testing, the subject naturally dropped his arm perpendicularly to the ground as shown in Fig. 14, regarded as the initial position. The device was programmed to drive the subject's arm to complete elbow flexion and extension in sequence with a range of 90°, which simulates a basic elbow rehabilitation procedure. Throughout the process, the subject's elbow movements were totally powered by the device. The reference trajectory was obtained from the motor encoder, while the actual trajectory of the subject's elbow joint was recorded by attaching an MTx sensor to the end of the output link.

To explore the power-assist behaviors along with variable stiffness actuation, five different levels of joint stiffness were selected by moving the pivot position to 0, 5, 10, 15, 20 mm respectively. The elbow power-assist movement was tested for each level of stiffness. This trial was repeated 10 times to obtain the mean angular error between the reference and the actual trajectory for 5 different levels of joint stiffness.

The trajectory results of the first elbow power-assist trial for the five levels of joint stiffness are shown in Fig. 15. The amplitude of elbow angle is varied with respect to the actuated joint stiffness. As we stated in Section 3, the output link can be deviated from its original equilibrium position by applying an external force. When the PVSED drives the subject to perform elbow flexion and extension, due to the weight of the subject's arm, the output link worn by the user was separated with the main frame thereby resulting in an angular error between the reference and the actual angular trajectory. The angular error is apparent in low joint stiffness. With increasing elbow joint stiffness, the actual trajectory gets closer to the reference trajectory. The mean values of the angular error for ten trials are

Table 7 Compensated stiffness K

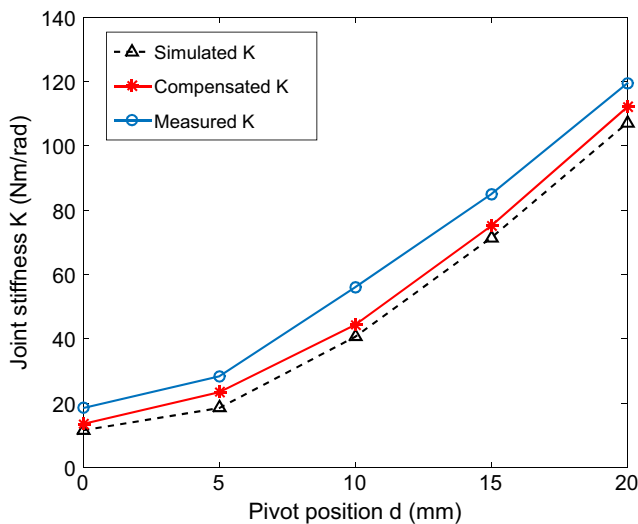| Pivot Position d (mm)	Compensated K (Nm/rad)	RMSE (Nm/rad)
0	13.55	0.91
5	23.41	0.97
10	44.34	2.13
15	75.14	1.87
20	112.09	1.21

Fig. 13 Joint stiffness versus pivot position. Simulated, compensated and measured stiffness show a significant tendency that the elbow joint stiffness becomes higher with the increase of the pivot position

reported in Fig. 16. By regulating the pivot position from 0 mm to 20 to increase the joint stiffness, the angular error was reduced from 16.97° to 1.68°. Actuated in a lower joint stiffness, the PVSED can provide compliant assistance to the human elbow, which allows relatively large deviations from its desired position so as to avoid excessive interaction forces and passively ensure the user's safety. With the increase of joint stiffness, the angular difference between the reference and the actual trajectory is decreased. Therefore, the rehabilitation intensity can be improved by increasing the joint stiffness. By means of the integrated VSA, the PVSED is capable of adjusting the actuated elbow joint stiffness in accordance with the specific impairment level of the patient's upper limb.
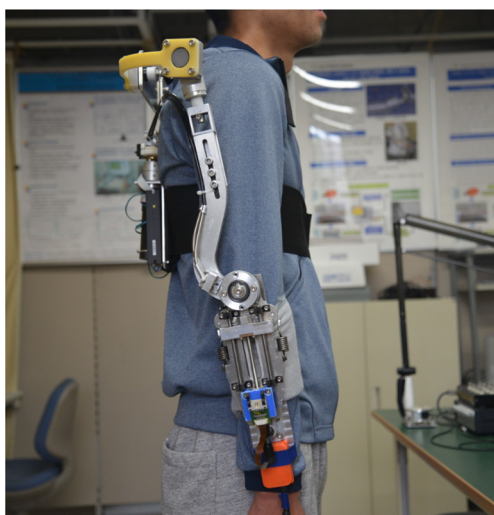

Fig. 14 Experimental setups. The subject naturally dropped his arm perpendicularly to the ground where is regarded as the initial position. An MTx sensor is attached to the end of the output link to record the actual trajectory of the elbow movements
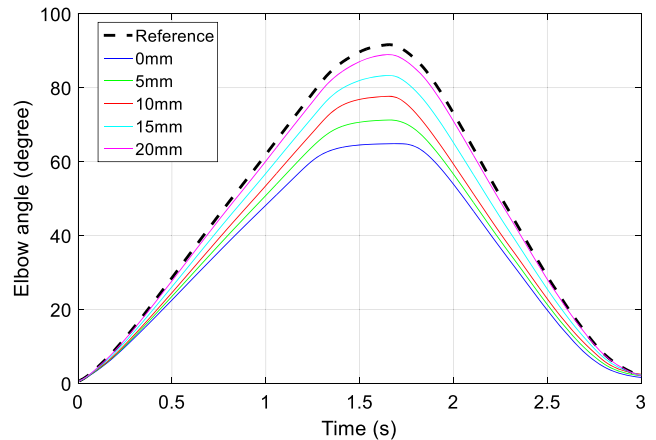

Fig. 15 Elbow rehabilitation task. By increasing the elbow joint stiffness, the actual trajectory gets closer to the reference trajectory

5 Discussion

Powered exoskeletons can provide independent assistance to specific joints according to the training requirements (Song and Guo 2012). This characteristic significantly improves the rehabilitation training for the patients with specific upper limb impairments. Since safety and comfort are important factors for robot-aided rehabilitation, some researchers have attempted to build comfortable kinematic structures and safe actuation systems for wearable rehabilitation devices. Vitiello et al. (2013) proposed an elbow exoskeleton NEUROExos, which is powered by an antagonistic-driven compliant joint (ADCJ). The device can acquire compliance control for a robot-in-charge rehabilitation mode and near-zero impedance torque control for a patient-in-charge rehabilitation mode. However, the spring characteristic of the ADCJ is required
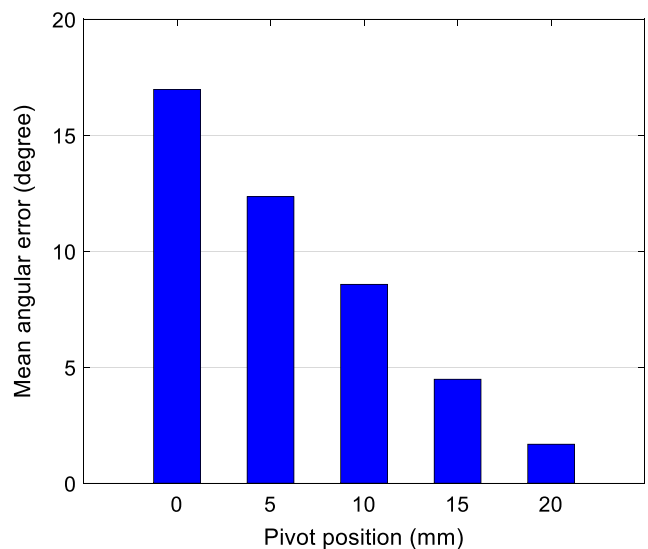

Fig. 16 Trajectory error between the reference and the actual trajectory. With the increase of elbow joint stiffness, the trajectory error is decreased evidently

to be linear by using two antagonistic non-linear springs for stiffness variation, which resulted in the complex mechanical structure and difficulties in regard to stiffness variation. Song et al. (2014) developed a light-weight upper limb exoskeleton rehabilitation device (ULERD) and implemented resistance training for the elbow joint by a closed-loop impedance control. However, the actuator is inherently rigid and the resistance adjustment can only be achieved by means of complicated closed-loop interaction control strategies. The impedance control will lose effect once beyond the control bandwidth and the system will regain high inherent impedance that may threaten the wearer's safety. To passively ensure a safe rehabilitation process without complicated control algorithms, Zhang et al. (2017) proposed an upper limb rehabilitation device with an integrating compliant actuator and a torque limiter mechanism. The compliance of the actuation system is achieved by the integrated compliant actuator. In addition, once the interaction force exceeds the predefined safety threshold, the output actuator will be released by the torque limiter mechanism to avoid any overload on the human arm. However, the application of this device is limited due to its 1-DOF kinematic structure, which restrains the patient's natural joint ROM. Additionally, it must be fixed in a stationary place and the user has to adjust his/her body position to adapt to the human-robot interface, which is extremely inconvenient for stroke patients with impaired upper limbs.

Different from the aforementioned devices, this paper presents a novel powered exoskeleton device PVSED which ensures the user's natural joint ROM and adjusts the joint stiffness independently. It is a portable and wearable device for elbow rehabilitation. The backpack-like design makes it possible to carry the PVSED on the wearer's back and thus greatly expands its support for daily living. There are 3 passive shoulder DOFs and 2 length adjustment DOFs to ensure the joint ROM and the intra-subject variability. More importantly, for guaranteeing sufficient torque for rehabilitation while keeping a safe human-robot interaction, a VSA is integrated into the device for independent stiffness adjustment. The stiffness variation is passively achieved by moving the pivot position, which simplifies the mechanical structure and does not require any closed-loop interaction control strategy.

The PVSED is expected to assist neurological patients with impaired arms to perform safe and comfortable rehabilitation training. The portable design facilitates home-based rehabilitation setups and allows for use outside of the home. In order to adapt to those patients with specific upper limb impairment levels, the PVSED can regulate the actuated joint stiffness to provide appropriate assistance for elbow rehabilitation. From this variable-stiffness characteristic, the PVSED also has the potential to gradually promote the intensity of rehabilitation training for chronic hemiparetic stroke survivors.

While these are significant advantages and promising functions, some limitations of this study need to be noted and addressed in the near future. Firstly, it was noted in Fig. 12 that the measured stiffness suffered backlash, which resulted in an inflection point in the force-deflection diagram. The backlash is caused by the internal characteristic of the cable, which is inevitable for cable-driven devices (Agrawal et al. 2010). Although we applied a linear fitting method to measure the actual stiffness and circumvented the backlash effect by linearly approximating the portion of the curve after the inflection point, these methods cannot eliminate or reduce the inherent backlash. To some extent, a higher cable tension can restrain the backlash effect but a solution based on the adaptive control strategy is preferred to compensate for the backlash effect. Secondly, a passive rehabilitation training movement in which the device drives the user's upper limb was tested in the experiment. The movement is totally powered by the device based on a position control strategy. In order to promote gradual active participation by the patient, active rehabilitation training in which the user drives the device to perform movement training is a promising training method. For realizing active rehabilitation training, a closed-loop torque control is desired to provide an "assist-as-needed" torque field to help the patients complete the task-oriented rehabilitation. Thirdly, the preliminary functionality of the PVSED was evaluated on a healthy subject. Rehabilitation trials on post-stroke patients are expected to further assess its feasibility in the future.

6 Conclusion

In this paper, we presented the design and preliminary evaluation of a powered variable-stiffness exoskeleton device which focuses on home-based elbow rehabilitation for post-stroke patients. It has the following notable features. Firstly, the portable, compact structure enables its use in daily living without undue burden. Secondly, passive human-motion controlled DOFs and frame adjustment DOFs ensure a desired kinematic compatibility between the exoskeletal and human joint for the people with different body sizes. Thirdly, the PVSED is capable of adjusting the assistance levels for the patients' elbow rehabilitation training by means of an integrated VSA.

Preliminary experiments were carried out to characterize the integrated VSA and evaluate the functionality of the proposed PVSED. The VSA characteristic experiment showed that by moving the pivot position, the actuated elbow joint stiffness can be adjusted independently. Futhermore, an elbow power-assist testing for different levels of joint stiffness was carried out on a healthy subject. The trajectory results showed that different angular error levels with respect to the reference trajectory appeared for the five levels of joint stiffness. More importantly, the angular error was reduced by applying a higher joint stiffness. With the proper choice of joint stiffness,

the PVSED can provide suitable training intensity for the patient with specific upper limb impairment levels.

Future work will focus on eliminating the backlash effect and promoting "assist-as-needed" active rehabilitation training based on closed-loop torque control strategies. Attention will also be devoted to carrying out post-stroke rehabilitation trials.

References

M. Abe, N. Yamada, Modulation of elbow joint stiffness in a vertical plane during cyclic movement at lower or higher frequencies than natural frequency. Exp. Brain Res. **153**(3), 394–399 (2003)

V. Agrawal, W. Peine, B. Yao, S. Choi, *Control of cable actuated devices using smooth backlash inverse.* IEEE International Conference on Robotics and Automation (ICRA). 1074–1079 (2010)

M. Babaiasl, S. Mahdioun, P. Jaryani, M. Yazdani, A review of technological and clinical aspects of robot-aided rehabilitation of upper-extremity after stroke. Disabil. Rehabil. Assist. Technol. **11**(4), 263–280 (2016)

S. Barreca, S. Wolf, S. Fasoli, R. Bohannon, Treatment interventions for the paretic upper limb of stroke survivors: A critical review. Neurorehabil. Neural Repair **17**(4), 220–226 (2003)

S. Groothuis, G. Rusticelli, A. Zucchelli, S. Stramigioli, R. Carloni, The variable stiffness actuator vsaut-ii: Mechanical design, modeling, and identification. IEEE/ASME Trans. Mechatron. **19**(2), 589–597 (2014)

S. Hesse, G. Schulte-Tigges, M. Konrad, A. Bardeleben, C. Werner, Robot-assisted arm trainer for the passive and active practice of bilateral forearm and wrist movements in hemiparetic subjects. Arch. Phys. Med. Rehabil. **84**(6), 915–920 (2003)

G. Kwakkel, B. Kollen, H. Krebs, Effects of robot-assisted therapy on upper limb recovery after stroke: A systematic review. Neurorehabil. Neural Repair **22**(2), 111–121 (2008)

X. Li, Y. Pan, G. Chen, H. Yu, Adaptive human–robot interaction control for robots driven by series elastic actuators. IEEE Trans. Robot. **33**(1), 169–182 (2017)

A. Lo, P. Guarino, L. Richards, J. Haselkorn, G. Wittenberg, D. Federman, B. Volpe, Robot-assisted therapy for long-term upper-limb impairment after stroke. N. Engl. J. Med. **362**(19), 1772–1783 (2010)

P. Lum, C. Burgar, P. Shor, M. Majmundar, M. Van der Loos, Robot-assisted movement training compared with conventional therapy techniques for the rehabilitation of upper-limb motor function after stroke. Arch. Phys. Med. Rehabil. **83**(7), 952–959 (2002)

P. Maciejasz, J. Eschweiler, K. Gerlach-Hahn, A. Jansen-Troy, S. Leonhardt, A survey on robotic devices for upper limb rehabilitation. J. Neuroeng. Rehabil. **11**(1), 3 (2014)

D. Mozaffarian, E. Benjamin, A. Go, D. Arnett, M. Blaha, M. Cushman, H. Fullerton, Executive summary: Heart Disease and Stroke Statistics-2016 update: A report from the American Heart Association. Circulation **133**(4), 447 (2016)

T. Nef, M. Guidali, R. Riener, ARMin III–arm therapy exoskeleton with an ergonomic shoulder actuation. Appl. Bionics Biomech. **6**(2), 127–142 (2009)

N. Norouzi-Gheidari, P. Archambault, J. Fung, Effects of robot-assisted therapy on stroke rehabilitation in upper limbs: systematic review and meta-analysis of the literature. J. Rehabil. Res. Dev. **49**(4), 479 (2012)

J. Patton, M. Stoykov, M. Kovic, F. Mussa-Ivaldi, Evaluation of robotic training forces that either enhance or reduce error in chronic hemiparetic stroke survivors. Exp. Brain Res. **168**(3), 368–383 (2006)

J. Perry, J. Rosen, S. Burns, Upper-limb powered exoskeleton design. IEEE/ASME Trans. Mechatron. **12**(4), 408–417 (2007)

B. Siciliano, O. Khatib, *Springer handbook of robotics*: Springer (2016)

Z. Song, S. Guo, Design process of exoskeleton rehabilitation device and implementation of bilateral upper limb motor movement. J. Med. Biol. Eng. **32**(5), 323–330 (2012)

Z. Song, S. Guo, M. Pang, S. Zhang, N. Xiao, B. Gao, L. Shi, Implementation of resistance training using an upper-limb exoskeleton rehabilitation device for elbow joint. J. Med. Biol. Eng. **34**(2), 188–196 (2014)

A. Stienen, E. Hekman, F. Van Der Helm, H. Van Der Kooij, Self-aligning exoskeleton axes through decoupling of joint rotations and translations. IEEE Trans. Robot. **25**(3), 628–633 (2009)

R. Van Ham, T. Sugar, B. Vanderborght, K. Hollander, D. Lefeber, Compliant actuator designs. IEEE Robot. Autom. Mag. **16**(3) (2009)

G. Vanpee, G. Hermans, J. Segers, R. Gosselink, Assessment of limb muscle strength in critically ill patients: A systematic review. Crit. Care Med. **42**(3), 701–711 (2014)

L. Visser, R. Carloni, S. Stramigioli, Energy-efficient variable stiffness actuators. IEEE Trans. Robot. **27**(5), 865–875 (2011)

N. Vitiello, T. Lenzi, S. Roccella, S. De Rossi, E. Cattin, F. Giovacchini, M. Carrozza, NEUROExos: A powered elbow exoskeleton for physical rehabilitation. IEEE Trans. Robot. **29**(1), 220–235 (2013)

S. Wolf, G. Grioli, O. Eiberger, W. Friedl, M. Grebenstein, H. Höppner, M. Catalano, Variable stiffness actuators: Review on design and components. IEEE/ASME Trans. Mechatron. **21**(5), 2418–2430 (2016)

H. Yu, S. Huang, G. Chen, N. Thakor, Control design of a novel compliant actuator for rehabilitation robots. Mechatronics **23**(8), 1072–1083 (2013)

H. Yu, S. Huang, G. Chen, Y. Pan, Z. Guo, Human–robot interaction control of rehabilitation robots with series elastic actuators. IEEE Trans. Robot. **31**(5), 1089–1100 (2015)

S. Zhang, S. Guo, M. Pang, B. Gao, P. Guo, Mechanical design and control method for sea and VSA-based exoskeleton devices for elbow joint rehabilitation. Neuro Biomed Eng **2**(3), 142–147 (2014)

S. Zhang, S. Guo, Y. Fu, L. Boulardot, Q. Huang, H. Hirata, H. Ishihara, Integrating compliant actuator and torque limiter mechanism for safe home-based upper-limb rehabilitation device design. J. Med. Biol. Eng. **37**(3), 357–364 (2017)